Proceedings of the ASME 2020 Dynamic Systems and Control Conference
DSCC2020
October 4-7, 2020, Pittsburgh, PA, USA

DSCC2020-3183

MARKER BASED ROW ALIGNMENT CONTROL FOR AN AGRICULTURAL SCOUTING ROBOT

Qiang Li, Xiangling Kong[1,2], Yunjun Xu[2]
Department of Mechanical and Aerospace Engineering
University of Central Florida
Orlando, Florida, USA

ABSTRACT

In recent years, autonomous robots have been gradually introduced into various agricultural operations to address the ever-increasing labor shortage problem. Accurate navigation from one row to another is one of the many challenging tasks for an autonomous robot scouting in semi-structured agricultural fields. In this study, a marker-based row alignment control is proposed for the cross-bed motion of a scouting robot in strawberry fields. Specifically, a feature-based computer vision algorithm is used to detect primitive markers placed at the end of each planting bed. Then the image coordinates of detected markers are used to guide the robot to move away from one row and then align with the next one. The proposed method is low cost and robust with respect to varying lighting conditions, and has been validated in a local strawberry farm.

Keywords: perception, motion control, agricultural robot

1 INTRODUCTION

According to the United Nations, the human population will be around 9.7 billion in 2050 [1] and the food demand is expected to be 60% higher than it is today [2]. Yet in some of the most populated areas in the world, the percentage of working-age population will drop as much as 20% in the next 50 years. On the other hand, climate change, pollution, over-fertilization, and land degradation are threatening our remaining cultivable lands. Precision agriculture emerges with the perspective of increasing the yields with limited resources. Aided with autonomous agricultural robots, it prospects to mitigate the effect of human labor shortage as well.

Agricultural robots are commonly tasked to navigate through the fields and conduct disease detection, harvesting, or phenotyping. Two motion primitives in semi-structured fields like strawberry fields are: over-bed motion and cross-bed motion. The over-bed motion refers to the robot moving along the planting bed, while the cross-bed motion refers to the robot transferring between adjacent planting beds. The challenge lies in achieving centimeter navigation accuracy at a manageable cost. Global positioning system (GPS) was promising to provide a guidance solution for agricultural robots. With the prevalence of Real Time Kinematics (RTK) technologies, RTK GPS based centimeter accuracy positioning [3] becomes affordable. Yet this method has seldomly been implemented because all headlands and turning points in a field need to be geo labeled beforehand. Considering the fact that the number of such landmarks varies dramatically between different fields, the workload to implement such a system can be prohibitive.

Vision-based methods have been widely used on indoor robotic applications, such as picking or sorting packages [4], assisting medical surgery operations [5], and indoor navigations [6]. Researchers have also investigated vision based techniques for outdoor applications. For example, a color-system combined with a Photonic Mixer Device is used on a harvesting robot to help an end-effector locate apples [7]. A color-based vision system is developed to control a weeding tool to remove weeds [8]. Nevertheless, using vision techniques to guide a robot through a field is still a hurdle, mainly because of the divergent terrain types and different weather/lighting conditions.

In our previous study [9], an ultrasonic sensor based proportional-integral-derivative (PID) controller and a vision based nonlinear robust controller were designed to help a field robot accomplish over-bed motion and cross-bed motion, respectively. In the cross-bed motion control, the robot uses webcams to find and follow the centerlines of beds. The field tests show some encouraging results. However, the proposed method is not robust with respect to different weather conditions or light intensities in the outdoor environment. For example, the cameras have to be manually re-calibrated if the weather changes from sunny to cloudy. The thresholds for the color channels must be manually adjusted when the light changes, e.g., when the sun

[1] Contact author: xl.kong@knights.ucf.edu
[2] Member of ASME

gets covered by the clouds. Besides, some strawberry beds are neither straight nor even in width, leading to inaccurate detection of the bed centerlines.

This study is an extension of Ref. [9] aiming to improve the robustness of cross-bed motion control with respect to light intensity and weather condition. A simple marker-based row alignment control algorithm is proposed for the cross-bed motion. First, a color-ratio index [10] based computer vision algorithm with an auto exposure adjustment is developed to extract the markers from the background. Secondly, a vision-based PID controller is designed to help the robot align with the target row. The proposed method is validated via experiments in a commercial strawberry farm. Compared with the method in Ref. [9], the algorithm can automatically adjust the exposure settings of the camera, avoid repetitive calibrations under different weather conditions, and is robust with respect to varying bed conditions.

This paper is organized as follows. The problem is defined in Section 2. In Section 3, a marker based row alignment control algorithm is proposed, which includes three parts: a feature-based marker detection method, the proof of necessary and sufficient conditions for the vision-based row alignment, and the design of the marker-based cross-bed control algorithm. In Section 4, the robot system is introduced, and the experiment results are presented. Conclusions are given in the end.

2 PROBLEM DEFINITION

The motion connecting two neighboring beds is referred as the cross-bed motion. The marker-based cross-bed motion control has three phases as shown in Figure 1. In Phase 1, the robot uses the right camera to align with Marker I. In Phase 2, the robot moves toward Bed II for a predefined distance and then uses the side camera to align with Bed II. In Phase 3, the robot turns 90° and uses the front camera to align with Marker II while entering Bed II.

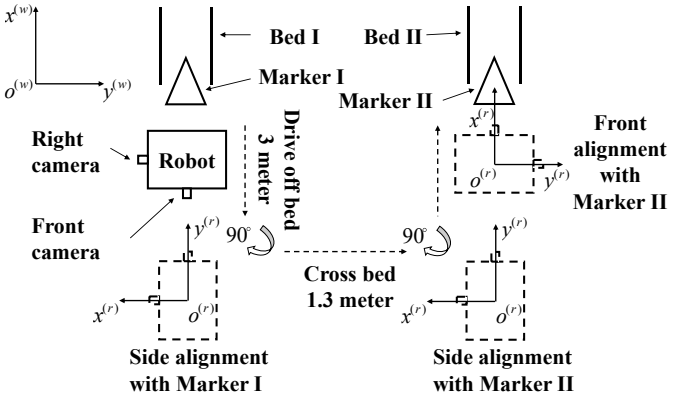

Figure 1. The cross-bed motion of the robot in a two-bed experiment

To achieve the marker-based crossing bed motion, two algorithms are designed. First, an image processing algorithm is designed to extract the markers from the background in real time. Secondly, a marker-based cross-bed control algorithm is developed to guide the robot to enter the neighboring bed. The motion of the ground robot is governed by [11] as

$$\begin{bmatrix} \dot{x}_{bot}^{(w)} \\ \dot{y}_{bot}^{(w)} \\ \dot{\psi} \end{bmatrix} = \begin{bmatrix} \cos\psi & 0 \\ \sin\psi & 0 \\ 0 & 1 \end{bmatrix} \begin{bmatrix} v \\ \omega \end{bmatrix} \tag{1}$$

where $x_{bot}^{(w)}$ and $y_{bot}^{(w)}$ are the robot position in the world frame defined in Figure 1, and ψ is the heading angel. v and ω are the speed and the angular velocity of robot, respectively.

3 MARKER BASED MOTION CONTROL

The marker-based cross-bed algorithm controls the transition and rotation of the robot to transit from the current bed to the next one and align with it both laterally and longitudinally.

3.1 Feature-based Marker Detection

Three features are considered when designing the marker: shape, color, and size. An equilateral triangle shaped flat marker made from red antiglare material is designed and installed at the end of each strawberry bed. The equilateral triangle shape is chosen for the fact that, based on the projection relationship, the median of the bottom side is perpendicular to the bottom side only when it is viewed straight. The red color is chosen to distinguish the marker from the green plants and black plastic films used to cover the beds, both of which resembles the marker in shape. The size of the marker is chosen so that it is sizable for feature extraction, yet not oversized for the ground clearance of the robot.

The marker is installed at an upward inclination angle of approximately 60°, so that the robot can capture enough features whether it is away from or close to the bed. On the other hand, the camera aboard the robot is installed at a downward elevation angle that is fine-tuned to provide an unobstructed view of the marker from a wide range of distance. The bottom median of the marker is aligned with the orientation of the strawberry bed. Figure 2 shows an installed marker at the end of a strawberry bed.

Figure 2. Demonstration of the marker in the strawberry field

A feature based computer vision algorithm (shown in Figure 3) is used to detect the marker features and extract it from the background. First, a color-ratio index based color filter is used to extract the red layer from the image. The uniqueness of this color-ratio index is the light scene invariance. Then, the features of a triangle are used to detect all triangles in the red layer. At last, one of the detected objects that resides closest to the

predicted location of the marker, meeting a predefined size criterion, is qualified as the extracted marker image.

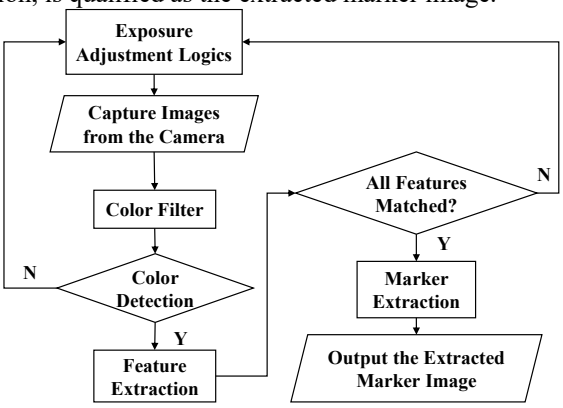

Figure 3. Feature based marker extraction algorithm

Lighting condition is a major challenge when applying vision-based algorithms in a field robot. The chosen antiglare material for the marker minimizes the effect of solar zenith angle and presents accurate color within a wide range of viewing angles. To ensure the marker is accurately exposed under various lighting conditions, a computer vision algorithm utilizing the Matlab support package for USB webcams [12] is designed (shown in Figure 4) to automatically adjust the exposure settings (i.e., shutter speed and brightness) of the camera in case that an inaccurate exposure leads to a detection failure. Two overexposure ratio criteria are predefined that will direct the logic to whether yield a brighter image or a darker one. The criteria are chosen based on field test data. When the overexposure ratio falls between 0.1 and 0.3, the color filter is guaranteed to detect the color of the marker.

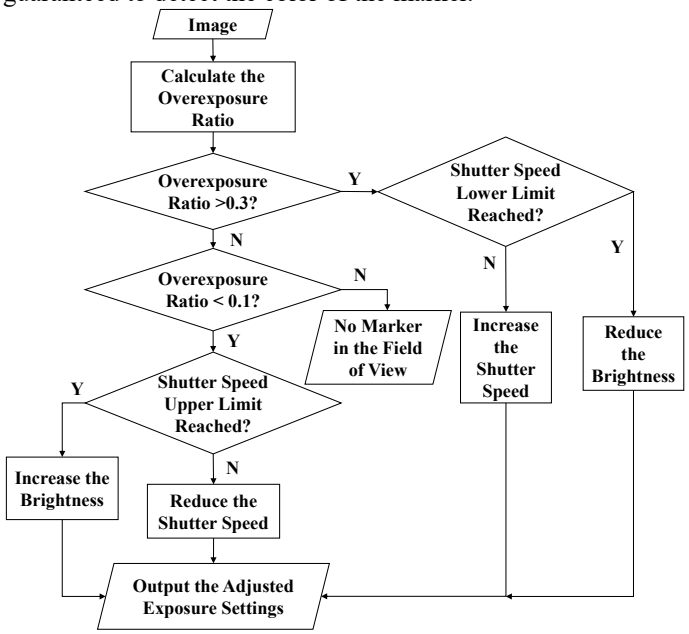

Figure 4. Automatic exposure adjustment algorithm

3.2 Row Alignment

The position and heading angle ψ of scouting robot are defined in the world frame Ω_I, as shown in Figure 5. The mass center of robot is chosen to be the origin point O_r of the robot frame. The original point O_c of the camera frame Ω_c is placed at the focal point of the camera.

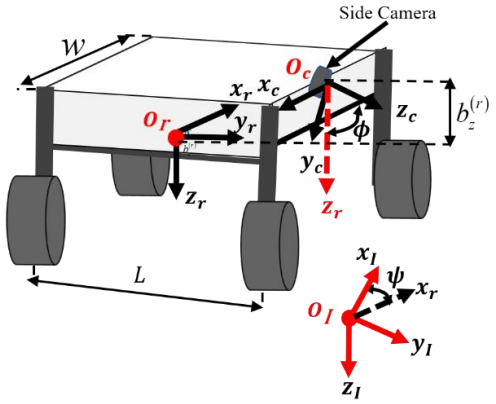

Figure 5. Coordinates of the scouting robot

Lemma 1: The robot aligns well with a point P in the world frame along the $\boldsymbol{x}_I$ direction if and only if P locates along the vertical centerline in the image plane of the camera onboard the robot.

Proof: Necessary condition: Assume that there is a ground point P in the world frame, such that $\boldsymbol{P}^{(w)} = \left[x_P^{(w)},\ y_P^{(w)},\ 0\right]^T$. The origin of robot frame in the world frame is $\boldsymbol{x}_{bot}^{(w)} = \left[x_{bot}^{(w)},\ y_{bot}^{(w)},\ z_{bot}^{(w)}\right]^T$, where $z_{bot}^{(w)}$ is the positional component along the $\boldsymbol{z}_I$ direction in the world frame, and is half of the robot height h_r. A camera is mounted on the robot with a fixed position bias $\boldsymbol{x}_{\mathbf{c}}^{(\mathbf{r})} = \left[0,\ w_r/2,\ -b_z^{(r)}\right]^T$ in the robot frame O_r and an elevation angle ϕ, where w_r is the width of the robot and $b_z^{(r)}$ is the position component along the $\boldsymbol{z}_r$ direction in the robot frame. The position of P in the robot frame can be calculated by

$$\boldsymbol{P}^{(r)} = R_z^{(r/w)}\left(\boldsymbol{P}^{(w)} + \boldsymbol{x}_{\mathbf{bot}}^{(w)}\right) \tag{2}$$

where $R_z^{(r/w)} \in \Re^{3\times3}$ is the rotation matrix from the world frame to the robot frame. The position of P in the camera frame is

$$\boldsymbol{P}^{(\mathbf{c})} = R^{c/r}\left(\boldsymbol{P}^{(r)} + \boldsymbol{x}_{\mathbf{c}}^{(r)}\right) \tag{3}$$

where $R^{c/r} \in \Re^{3\times3}$ is the rotation matrix from the robot frame to the camera frame. Finally, the pixel position of P in the image plane is

$$\boldsymbol{P}^{(p)} = K_c \boldsymbol{P}^{(c)} / z^{(c)} \tag{4}$$

where $z^{(c)}$ is the z component of $\boldsymbol{P}^{(c)}$ and K_c is the intrinsic matrix of the camera [13] as

$$K_c = \begin{bmatrix} f_x & 0 & c_x \\ 0 & f_y & c_y \\ 0 & 0 & 1 \end{bmatrix} \quad (5)$$

Here $[f_x, f_y]$ and $[c_x, c_y]$ are the focal length and focal point, which can be acquired by camera calibrations.

If point P is located along the line $x_p^{(w)} = 0$, i.e. $\boldsymbol{P}^{(w)} = \begin{bmatrix} 0, & y_p^{(w)}, & 0 \end{bmatrix}^T$, when the robot aligns well with P, such that $x_{bot}^{(w)} = 0$ and $\psi = 0°$, then according to Eq. (2), point P in the robot frame is

$$\boldsymbol{P}^{(r)} = \begin{bmatrix} \sin\psi\left(y_{bot}^{(w)} + y_p^{(w)}\right) \\ -\cos\psi\left(y_{bot}^{(w)} + y_p^{(w)}\right) \\ h_r/2 \end{bmatrix} = \begin{bmatrix} 0 \\ y_p^{(w)} - y_{bot}^{(w)} \\ h_r/2 \end{bmatrix} \quad (6)$$

Point P in the camera frame by using Eq. (3) is

$$\boldsymbol{P}^{(c)} = \begin{bmatrix} 0, & y^{(c)}, & z^{(c)} \end{bmatrix}^T \quad (7)$$

where $y^{(c)} = -\sin\phi\left(w_r/2 + y_{rot}^{(w)} - y_p^{(w)}\right) - \cos\phi\left(b_z^{(r)} - h_r/2\right)$ and $z^{(c)} = \cos\phi\left(w_r/2 - y_{bot}^{(w)} - y_p^{(w)}\right) - \sin\phi\left(b_z^{(r)} - h_r/2\right)$.

The position of P in the image can then be calculated by using Eq. (4) as

$$\boldsymbol{P}^{(p)} = \begin{bmatrix} c_x \\ c_y - \left(f_y y^{(c)}\right)/z^{(c)} \end{bmatrix} \quad (8)$$

Therefore, when the robot aligns well, the target point P is along $x^{(p)} = c_x$ in the image plan, where $x^{(p)}$ is the positional component of $\boldsymbol{P}^{(p)}$ along the $\boldsymbol{x}$ direction of the image plane.

Sufficient Condition: Assume that there is a point P in the image plane, such that $\boldsymbol{P}^{(p)} = \begin{bmatrix} c_x, & c_y + b \end{bmatrix}^T$, where b is an offset distance along the $\boldsymbol{y}$ direction in the image plane, the distance between the camera to P can be measured as $z^{(c)}$, then the position of P in the camera frame can be calculated by

$$\boldsymbol{P}^{(c)} = K_c^{-1} \boldsymbol{P}^{(p)} z^{(c)} \quad (9)$$

Point P in the robot frame is

$$\boldsymbol{P}^{(r)} = \left(R^{(c/r)}\right)^{-1} \left(\boldsymbol{P}^{(c)} + \boldsymbol{x}_c^{(r)}\right) \quad (10)$$

Then Point P in the world frame is

$$\boldsymbol{P}^{(w)} = \left(R_z^{(r/w)}\right)^{-1} \left(\boldsymbol{P}^{(r)} + \boldsymbol{x}_{rob}^{(w)}\right) \quad (11)$$

Assume that the robot is straightly right, such that the heading angle $\psi = 0$, the position of P in the world frame is

$$\boldsymbol{P}^{(w)} = \begin{bmatrix} -x_{bot}^{(w)} \\ \cos\phi\left(z^{(c)} - b_z^{(r)}\right) - \sin\phi\left(w_r/2 + \left(z^{(c)} b\right)/f_y\right) - y_{bot}^{(w)} \\ h_r/2 + \cos\phi\left(w_r/2 + \left(z^{(c)} b\right)/f_y\right) + \sin\phi\left(z^{(c)} - b_z^{(r)}\right) \end{bmatrix} \quad (12)$$

If point P in the world frame is $\boldsymbol{P}^{(w)} = \begin{bmatrix} 0, & y^{(w)}, & 0 \end{bmatrix}^T$, the positional component of $\boldsymbol{P}^{(w)}$ when $\psi = 0$ in the $\boldsymbol{x}_I$ direction has to be zero, i.e. $x_{bot}^{(w)} = 0$.

Lemma 1 describes the necessary and sufficient conditions for the robot to align with a point along the $\boldsymbol{x}_I$ direction in the world frame. To make sure the robot is aligned with the strawberry bed, the robot needs to align with the median of bottom side of the marker. Therefore, Lemma 1 is extended to the following corollary.

Corollary 1: The robot aligns well with a line in the world frame if and only if the projections of two points on this line are on the centerline ($x^{(p)} = c_x$) of the image plane. In other words, the projection of the line should along the image centerline $x^{(p)} = c_x$.

Remark 1: The robot is equipped with 2 side cameras (right and left) and 1 front camera. The side cameras are used to conduct the side alignment, while the front camera is used for the front alignment. To be brief, only the proof of the left side camera of the robot has been fully addressed, while the proof of other cameras can be proven following the same procedure.

3.3 Marker-based Cross-Bed Motion Control

The image of a marker is illustrated in Figure 6, in which c is the center of the image, m_1 and m_2 are the bottom midpoint and the top vertex of the marker in the image plane, respectively. Let subscripts x and y denote their corresponding pixel coordinates. According to Corollary 1, to align the robot with the strawberry bed, the following error variable

$$\boldsymbol{e} \triangleq \begin{bmatrix} d^{(p)} & \theta \end{bmatrix}^T \quad (13)$$

should be driven to zero, where $d^{(p)}$ is the pixel distance between the center of the marker's bottom side and the center line of the image plane, which is calculated by

$$d^{(p)} = c_x - m_{1,x} \quad (14)$$

θ is the angle between the median of the marker's bottom side and the center line of the camera image, which is calculated by

$$\theta = \tan^{-1}\left[\left(m_{2,y} - m_{1,y}\right)/\left(m_{2,x} - m_{1,x}\right)\right] \quad (15)$$

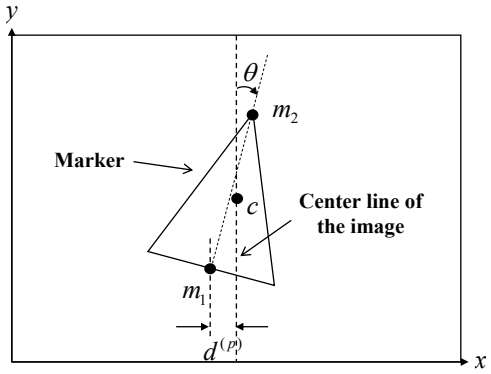

Figure 6. Illustration of a marker in the camera image plane

The motion of the robot is governed by the dynamic model given by (1). Under the assumption that the robot can perform 90° turns with an acceptable accuracy, the small angle assumption can be further established during the alignments. During the front alignment (Phase 3), the transitional speed v of the robot is set to be constant, and (1) can be simplified as

$$\begin{bmatrix} \dot{x}_{bot}^{(w)} \\ \dot{y}_{bot}^{(w)} \\ \dot{\psi} \end{bmatrix} = \begin{bmatrix} 1 & 0 \\ \psi & 0 \\ 0 & 1 \end{bmatrix} \begin{bmatrix} v \\ \omega \end{bmatrix} \tag{16}$$

The dynamic model of the robot during front alignment can be simplified as

$$\begin{bmatrix} \dot{y}_{bot}^{(w)} \\ \dot{\psi} \end{bmatrix} = \begin{bmatrix} 0 & v \\ 0 & 0 \end{bmatrix} \begin{bmatrix} y_{bot}^{(w)} \\ \psi \end{bmatrix} + \begin{bmatrix} 0 \\ \omega \end{bmatrix} \tag{17}$$

The error variable during the front alignment is $\boldsymbol{e}_f = \begin{bmatrix} d^{(p)} & \theta_f \end{bmatrix}^T$, where $\theta_f = -\psi$. The error system can be described by

$$\begin{bmatrix} \dot{d}^{(p)} \\ \dot{\theta}_f \end{bmatrix} = \begin{bmatrix} -k \cdot v & 0 \\ 0 & -1 \end{bmatrix} \begin{bmatrix} \theta_f \\ \omega \end{bmatrix} \tag{18}$$

where $k > 0$ is a parameter determined by the distance between the marker and the camera. Since v is constant during front alignment, the virtual control [14] to eliminate $d^{(p)}$ is θ_f, which we define as

$$\theta_{ref} = K_{p,y} \left(d^{(p)} + \frac{1}{T_{i,y}} \int d^{(p)} \mathrm{d}t + T_{d,y} \dot{d}^{(p)} \right) \tag{19}$$

We subsequently define $e_\theta = \theta_{ref} - \theta_f$ and the following controller is designed to reduce this error

$$\omega = K_{p,\theta} \left(e_\theta + \frac{1}{T_{i,\theta}} \int e_\theta \mathrm{d}t + T_{d,\theta} \dot{e}_\theta \right) \tag{20}$$

During the side alignment (Phase 2), we assume the change of the distance between the robot and the bed is neglectable. Then the dynamic model of the robot during side alignment can be simplified as

$$\begin{bmatrix} \dot{y}_{bot}^{(w)} \\ \dot{\psi} \end{bmatrix} = \begin{bmatrix} -1 & 0 \\ 0 & 1 \end{bmatrix} \begin{bmatrix} v \\ \omega \end{bmatrix} \tag{21}$$

The error variable is $\boldsymbol{e}_s = [d^{(P)}, \theta_s]^T$, where $\theta_s = 90^\circ - \psi$. The error system can be described as

$$\begin{bmatrix} \dot{d}^{(p)} \\ \dot{\theta}_s \end{bmatrix} = \begin{bmatrix} -k & 0 \\ 0 & -1 \end{bmatrix} \begin{bmatrix} v \\ \omega \end{bmatrix} \tag{22}$$

The following controller is designed for system (22)

$$v = K_{p,x} \left(d^{(p)} + \frac{1}{T_{i,x}} \int d^{(p)} \mathrm{d}t + T_{d,x} \dot{d}^{(p)} \right) \tag{23}$$

$$\omega = K_{p,\theta} \left(\theta_s + \frac{1}{T_{i,\theta}} \int \theta_s \mathrm{d}t + T_{d,\theta} \dot{\theta}_s \right) \tag{24}$$

4 EXPERIMENTAL VALIDATION

4.1 Experiment Settings

The experimental robot platform is a four-wheel ground robot that is equipped with two Microsoft Studio webcams respectively facing forwards and rightwards, one Arduino Mega board for motor control, and a laptop with a dual core 2GHz CPU for the marker-based motion control algorithm. The webcam model has an adjustable exposure value (EV) range of 14 stops (0 to -13) and a brightness range of 226 stops (30 to 255). Since the aperture of camera is not adjustable, the EV is directly associated with the shutter speed. The smaller the EV, the faster the shutter speed. In a two-bed experiment setting, two markers are installed at one end of two adjacent strawberry beds as shown in Figure 7.

Figure 7. The two-bed experiment setup

The proposed marker-based alignment method is applied in the experiment to control the robot to finish the cross-bed motion as shown in Figure 1. The robot starts at the end of Bed I in a gesture ready to drive off the bed and executes the following cross-bed operation sequence:

- Drive off the bed for a preset distance of 3 meters.
- Make a right turn of 90° to point the right camera to Bed I.
- Execute the side alignment with Marker I using the right camera.
- Drive across bed for 1.3 meters, which is the approximate distance between beds in the experiment strawberry field.
- Execute the side alignment with Marker II using the right camera.
- Make a right turn of 90° to point the front camera to Bed II.
- Execute the front alignment with Marker II using the front camera and drive towards Bed II at a preset speed of 0.2 m/s.

4.2 Experiment Results and Discussion

In the cross-bed sequence, the off-bed transition, the cross-bed transition, and the 90° turns are open-loop operations. The vision-based alignments eliminate the errors introduced in the open-loop procedures and prepare the robot for the subsequent procedures.

The experiment presented below was conducted between 2 and 3pm on a cloudy day. The webcams are initialized with an

EV of -5 and a brightness value of 100. After the off-bed transition and the subsequent 90° turn, the automatic exposure adjustment algorithm reduces the EV to -12 to accommodate the lighting condition. The initial error variable with respect to Marker I is $\boldsymbol{e}_s = \begin{bmatrix} -48.23\,px & 0^{\circ} \end{bmatrix}^T$, where "*px*" denotes the unit for pixels. The side alignment with Marker I is executed to achieve $\boldsymbol{e}_s = [0 \quad 0]^T$. Under the alignment control, the position error is steadily reduced to 0, while the angle error is maintained around 0 throughout the process, as shown in Figure 8.

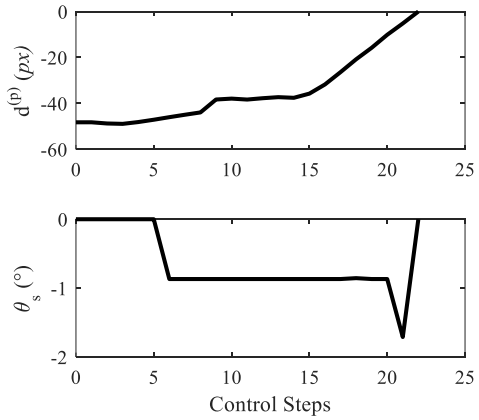

Figure 8. Changes of the error variables during the side alignment with Marker I

The robot then transits across these two beds. The error variable with respect to Marker II is $\boldsymbol{e}_s = \begin{bmatrix} 67.2\,px & 0.9548^{\circ} \end{bmatrix}^T$. During the side alignment with Marker II, the angle error is maintained close to 0, while the position error shows some oscillation, which mostly results from the rotation of the robot to eliminate the angle error. Changes of the error variables are shown in Figure 9.

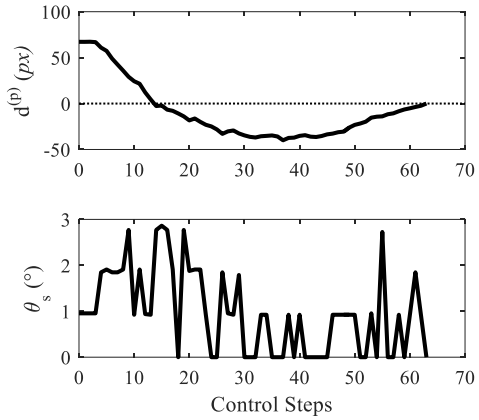

Figure 9. Changes of the error variables during side alignment with Marker II

After a 90° right turn to face Bed II, the robot carries out the front alignment with Marker II while transiting towards Bed II. The EV is increased to -11. The initial error variables with respect to Marker II is $\boldsymbol{e}_f = \begin{bmatrix} -122.17px & -4.76^{\circ} \end{bmatrix}^T$. As shown in Figure 10, the error variables steadily converge to 0, with slight oscillations occurring when the robot is very close to the bed where the ground is uneven.

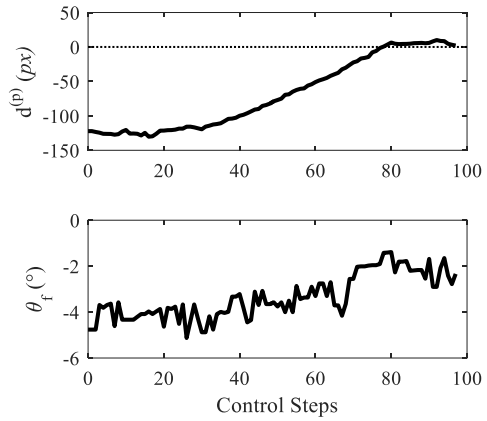

Figure 10. Changes of the error variables during front alignment with Marker II

We have conducted field tests on three cloudy and windy days. Our experiments usually extend from noon to late afternoon. The robot has flawlessly finished 11 uninterrupted cross-bed motions, all of which successfully connected two adjacent over-bed motions.

5 CONCLUSIONS

In this study, a simple marker-based row alignment control is proposed to enhance the performance of cross-bed motion of an agricultural robot in semi-structured fields. A robust feature-based matching algorithm is designed to detect the customized marker under varying outdoor conditions in real time. A vision-based alignment control algorithm is then developed to help the robot adjust its attitude and align with the target planting bed. Experiments are successfully conducted in a local strawberry farm.

ACKNOWLEDGEMENTS

The authors would like to acknowledge the National Science Foundation (#1924622) for the financial support. We would also like to thank Pappy's Patch, Oviedo FL for providing the experimental field.

REFERENCES

[1] United Nations, "World population prospects 2019," New York: United Nations, 2019.

[2] Hincks, J., "The world is headed for a food security crisis. Here's how we can avert it," *Time Magazine*, 2018.

[3] Wing, M. G., Eklund, A. and Kellogg, L. D., "Consumer-grade global positioning system (GPS) accuracy and reliability," *Journal of Forestry*, 2005, 103(4), pp.169-173.

[4] Li, L., Zhang, Y., Ripperger, M., Nicho, J., Veeraraghavan, M., and Fumagalli, A., "Autonomous object pick-and-sort

procedure for industrial robotics application," *International Journal of Semantic Computing*, 2019, 13(2), pp.161-183.
[5] Sultan, A. A., Samuel, L. T., Khlopas, A., Sodhi, N., Bhowmik-Stoker, M., Chen, A., Orozco, F., Kolisek, F., Mahoney, O., Smith, L., and Malkani, A., "Robotic-arm assisted total knee arthroplasty more accurately restored the posterior condylar offset ratio and the insall-salvati index compared to the manual technique; a cohort-matched study," *Surgical Technology International*, 2019, 34, pp.409-413.
[6] Gini, G. C. and Marchi, A., "Indoor robot navigation with single camera vision," *Proceedings of the 2nd International Workshop on Pattern Recognition in Information Systems*, 2002, 2, pp.67-76.
[7] Zhou, W., Feng, J., Liu, G. and Ma, X., "Application of image registration technology in apple harvest robot," *The Transactions of the Chinese Society of Agricultural Engineering*, 2013, 29(11), pp.20-26.
[8] Åstrand, B. and Baerveldt, A. J., "An agricultural mobile robot with vision-based perception for mechanical weed control," *Autonomous robots*, 2002, 13(1), pp.21-35.
[9] Freese, D.J. and Xu, Y., "Multiphase scouting control of an agricultural field robot with reachability analyses," *Journal of Dynamic Systems, Measurement, and Control*, 2019, 141(5), 051009 (12 pages)
[10] Kong, X. and Xu, Y., "Strawberry plant alive status detection and relative pixel based plant localization," *Journal of Dynamic Systems, Measurement, and Control*, 2020, 142(5), 054501 (6 pages).
[11] Laumond, J. P., Sekhavat, S. and Lamiraux, F., "Guidelines in nonholonomic motion planning for mobile robots," *Robot Motion Planning and Control*, Springer, Berlin, Heidelberg, 1998, pp.1-53.
[12] MathWorks, "Image acquisition toolbox: user's guide (R2015b)," Natick, Massachusetts: The MathWorks Inc., 2015.
[13] Zhang, Z., "A flexible new technique for camera calibration," *IEEE Transactions on Pattern Analysis and Machine Intelligence*, 2000, 22(11), pp.1330-1334.
[14] Kokotovic, P. V., "The joy of feedback: nonlinear and adaptive," *IEEE Control Systems Magazine*, 1992, 12(3), pp.7-17.